BIOCHEMISTRY
including biophysical chemistry & molecular biology

Article

pubs.acs.org/biochemistry

Binding Affects the Tertiary and Quaternary Structures of the *Shigella* Translocator Protein IpaB and Its Chaperone IpgC

Philip R. Adam,[†] Mrinalini K. Patil,[†] Nicholas E. Dickenson,[†] Shyamal Choudhari,[†] Michael Barta,[‡] Brian V. Geisbrecht,[‡] Wendy L. Picking,*[,†] and William D. Picking*[,†]

[†]Department of Microbiology and Molecular Genetics, Oklahoma State University, Stillwater, Oklahoma 74078, United States
[‡]School of Biological Sciences, University of Missouri—Kansas City, Kansas City, Missouri 64110, United States

Supporting Information

ABSTRACT: *Shigella flexneri* uses its type III secretion system (T3SS) to promote invasion of human intestinal epithelial cells as the first step in causing shigellosis, a life-threatening form of dysentery. The *Shigella* type III secretion apparatus (T3SA) consists of a basal body that spans the bacterial envelope and an exposed needle that injects effector proteins into target cells. The nascent *Shigella* T3SA needle is topped with a pentamer of the needle tip protein invasion plasmid antigen D (IpaD). Bile salts trigger recruitment of the first hydrophobic translocator protein, IpaB, to the tip complex where it senses contact with a host membrane. In the bacterial cytoplasm, IpaB exists in a complex with its chaperone IpgC. Several structures of IpgC have been determined, and we recently reported the 2.1 Å crystal structure of the N-terminal domain ($IpaB^{74.224}$) of IpaB. Like IpgC, the IpaB N-terminal domain exists as a homodimer in solution. We now report that when the two are mixed, these homodimers dissociate and form heterodimers having a nanomolar dissociation constant. This is consistent with the equivalent complexes copurified after they had been co-expressed in *Escherichia coli*. Fluorescence data presented here also indicate that the N-terminal domain of IpaB possesses two regions that appear to contribute additively to chaperone binding. It is also likely that the N-terminus of IpaB adopts an alternative conformation as a result of chaperone binding. The importance of these findings within the functional context of these proteins is discussed.

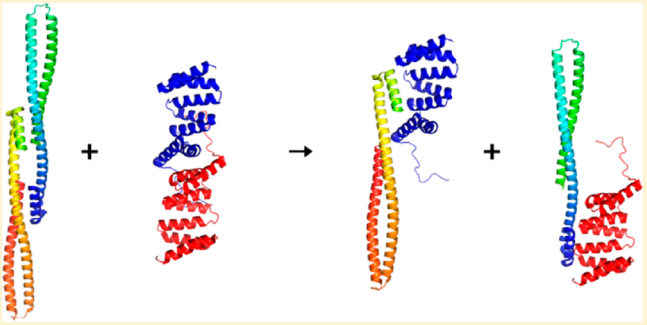

Type III secretion systems (T3SSs) are conserved virulence factors with diverse pathogen-specific roles used by a wide range of Gram-negative bacterial pathogens.[1,2] T3SSs are used to translocate effector proteins directly into a target cell's cytoplasm where they modulate a variety of host cell functions for the benefit of the pathogen.[3] *Shigella flexneri*, the causative agent of shigellosis, uses its T3SS to invade human colonic epithelial cells as an initial step in establishing infection.[3] Invasion is directed by the injection of effector proteins into the host cell cytoplasm that culminate in cytoskeletal rearrangements that ultimately result in pathogen uptake. Once inside the host cell, *Shigella* quickly lyses the vacuole to enter the cytoplasm where it replicates and spreads to adjacent cells by actin-based motility.[1−3]

The type III secretion apparatus (T3SA) is comprised of a basal body that spans the inner and outer bacterial membranes, a surface-exposed needle consisting of a polymer of the protein MxiH, and a secretion-controlling tip complex.[4−6] The nascent tip complex is composed of a pentameric ring of invasion plasmid antigen D (IpaD) at the exposed end of the T3SA needle.[4,7,8] Upon exposure to bile salts, IpaD undergoes a conformational change that leads to recruitment of the first hydrophobic translocator protein, IpaB, to the T3SA needle tip where it localizes distal to IpaD.[9] Induction of the T3SS occurs upon subsequent incubation with cholesterol-rich liposomes, which leads to recruitment of the second hydrophobic translocator protein, IpaC, to the needle tip where it associates with IpaB to ultimately form a translocon pore within the host cell membrane.[10] The newly formed translocon completes formation of a unidirectional conduit and promotes translocation of effectors from the bacterium directly into the host cell cytoplasm by the T3SS.[10]

Prior to their secretion, the translocator proteins IpaB and IpaC independently associate with their cognate class II chaperone IpgC in the *Shigella* cytoplasm.[11] Like all T3SS class II chaperones, IpgC is a small (17.8 kDa), highly α-helical protein with an acidic pI that possesses a tetratricopeptide repeat (TPR) fold.[11−15] Cytoplasmic association of the translocators with IpgC presumably occurs to prevent premature association of IpaB with IpaC and/or deleterious interaction of the translocators with the bacterial membrane.[11] Expression of the translocators in either *Shigella* or *Escherichia coli* in the absence of IpgC results in their rapid degradation.[11,16] Following delivery of the translocators to

Received: February 22, 2012
Revised: April 11, 2012
Published: April 12, 2012

ACS Publications © 2012 American Chemical Society

dx.doi.org/10.1021/bi300243z | *Biochemistry* 2012, 51, 4062−4071

the ATPase of the T3SA secretion platform in the *Shigella* cytoplasm, the released IpgC has been reported to form a dimer that associates with MxiE.[11] This MxiE−IpgC complex then acts as a transcription factor by binding DNA sequences at MxiE boxes to promote expression of late T3SS effector protein genes.[11]

Full-length IpaB can be produced in large amounts as a recombinant protein in *E. coli*, but only when co-expressed with IpgC.[16] Although the resulting IpaB−IpgC complex can be dissociated by incubation with certain mild detergents, this dissociation is not reversible. This could be a result of IpaB adopting a new conformation upon release from the chaperone because it forms discrete multimeric complexes in the absence of IpgC (data not shown). Some groups have proposed that a short peptide-length region of IpaB accounts for much of its interaction with IpgC and gives rise to a complex containing one IpaB and two IpgC molecules.[12,17] In this study, we examined the interaction of the N-terminal domain of IpaB with IpgC and used information about the structure of this IpaB domain to more precisely define the molecular basis for its chaperone binding. The hydrophobic nature of full-length IpaB has made a high-resolution structure elusive; however, the stabilizing effect of IpgC on IpaB has allowed us to determine the structure of its N-terminal domain.[18] Using this structure, we have found a useful starting point for understanding the intricacies of IpaB structure and the effect that IpgC binding has on it. In return, we have also been able to identify how IpaB binding influences the physical state of IpgC in solution. The implications of these findings in light of the known roles of IpaB and IpgC following induction of type III secretion are discussed.

EXPERIMENTAL PROCEDURES

Cloning, Expression, and Purification of Recombinant Proteins. The full-length *ipaB* gene was cloned into pT7HMT.[19] This vector was cotransformed with *ipgC* in pACYC-DUET[16] into *E. coli* BL21(DE3) and grown in Terrific Broth containing kanamycin (50 μg/mL) and chloramphenicol (30 μg/mL) at 37 °C to an absorbance at 600 nm (A_{600}) of ∼0.8. Protein co-expression and purification were as previously described.[18]

Individual DNA fragments encoding specific N-terminal fragments of IpaB (residues 1−94, 1−226, and 28−226) were designed, amplified by polymerase chain reaction, and subcloned into the pT7HMT plasmid. Each fragment of IpaB was also overexpressed from a modified version of the pT7HMT vector, described previously,[20] which encodes a Cys residue as the first (N-terminal) amino acid of the polypeptide and a second version that encodes Cys as the last (C-terminal) residue. Overexpression and purification of the translocator fragments were conducted as previously described for the IpaB−IpgC complex,[18] with the exception that recombinant TEV protease was used to digest the fusion affinity tag from each target protein.[21] Proteins were dialyzed against 10 mM phosphate (pH 7.4) with 150 mM NaCl (PBS) and used immediately or stored at −80 °C.

Fluorescence Labeling of Proteins. IpaB$^{N28.226}$, IpaB$^{C28.226}$, and IpaB$^{N1.226}$ contained a single Cys residue at either the N- or C-terminus. These IpaB fragments were dialyzed against labeling buffer [50 mM Hepes (pH 7.0), 150 mM NaCl, and 5 mM tris(2-carboxyethyl)phosphine (TCEP)]. The TCEP concentration was then reduced to 1 mM by dialysis prior to labeling with a 10-fold molar excess of AlexaFluor-350 maleimide (Alexa350) or fluorescein maleimide (FM) dissolved in dimethyl sulfoxide (DMSO) or *N*′,*N*′-dimethylformamide (DMF), respectively. Reaction mixtures were stirred under nitrogen for 2 h at 25 °C. Unreacted dye was removed by gel filtration using a Superdex-75 gel filtration column (GE Lifesciences) equilibrated with PBS. Alexa350-IpaB$^{C1.226}$ was unstable and could not be used in this study.

Far-UV Circular Dichroism (CD) Spectroscopy. Far-UV CD spectra were recorded on a Jasco model J-815 spectropolarimeter equipped with a Peltier temperature controller (Jasco Inc., Easton, MD).[22] Spectra were acquired using a 0.1 cm path-length quartz cuvette at 10 °C with a spectral resolution of 1.0 nm, a scanning rate of 50 nm/min, and a data integration time of 2 s. All spectra are an average of three measurements. Secondary structure thermal stability was monitored at 222 nm over a temperature range from 10 to 85 °C. Data were acquired every 2.5 °C, and the temperature ramp rate was 15 °C/h. The protein concentration was 0.3 mg/mL for IpaB and the IpaB−IpgC complex in 20 mM citrate-phosphate buffer (pH 7.0) with 150 mM NaCl. CD signals were converted to mean residue molar ellipticities $[\theta]_R$, and thermal transitions were analyzed using the Jasco Spectral Manager.

Fluorescence Polarization (FP). FM-IpaB$^{N28.226}$, FM-IpaB$^{C28.226}$, FM-IpaB$^{N1.226}$, and FM-IpaB$^{C1.226}$ were maintained at a concentration of 80 nM in PBS while IpgC was titrated in at concentrations ranging from 0 to 1 μM. After a 1 h incubation at room temperature, the FP of fluorescein was measured using an excitation wavelength of 485 nm and an emission wavelength of 520 nm in a Molecular Devices SpectraMax M5 plate reader. The FP of W105 was measured using an excitation wavelength of 295 nm and an emission wavelength of 340 nm.

Förster Resonance Energy Transfer and the Calculation of Intramolecular Distances. Fluorescence spectra were recorded using a Jobin-Yvon FluoroMax-4 spectrofluorometer based on nonradiative transfer of donor excitation energy from the native W105 to the Alexa350 acceptor of Alexa350-IpaB$^{N28.226}$, Alexa350-IpaB$^{C28.226}$, and Alexa350-IpaB$^{N1.226}$ fragments. Identical concentrations of donor only (D) samples (without the Alexa350 probe) or donor and acceptor (DA) samples (with the Alexa350 probe) were excited at 295 nm, and emission spectra were recorded from 300 to 400 nm. Excitation and emission slits were set to 2.5 nm, and the integration time was 1 s. Emission spectra of samples containing 1 μM Alexa350-IpaB$^{N28.226}$, Alexa350-IpaB$^{C28.226}$, and Alexa350-IpaB$^{N1.226}$ and either 0 or 1 μM IpgC were then collected. For the reported experiments, the acceptor labeling efficiency approached 100%.

The distance between the Trp donors and the Alexa350 acceptors was calculated on the basis of determined FRET efficiency values, which were measured spectrophotometrically and calculated by the quenching of donor fluorescence emission. The donor only spectra in each case were obtained using the IpaB fragment lacking an Alexa350 acceptor. The FRET efficiencies were calculated by[23]

$$E = 1 - \frac{F_{DA}}{F_D} \quad (1)$$

where E is the energy transfer efficiency, F_{DA} is the peak fluorescence intensity of the donor emission in the presence of the acceptor, and F_D is the peak fluorescence intensity of the

dx.doi.org/10.1021/bi300243z | *Biochemistry* 2012, 51, 4062−4071

donor emission in the absence of the acceptor fluorophore. From the energy transfer efficiencies, the distances of single donor−acceptor pairs can be calculated by[23]

$$r = R_0\left(\frac{1}{E} - 1\right)^{1/6} \quad (2)$$

where r is the distance between the FRET pair fluorophores, E is the measured energy transfer efficiency calculated from eq 1, and R_0 is the Förster distance specific for the FRET pair. The R_0 value for Trp as the donor and Alexa350 as the acceptor is reported to be 21 Å.[24] Though possible donor−acceptor distances for the IpaB N-terminal domain are discussed here, reliable determinations were only possible when the fluorescent IpaB species were not dimerized because the presence of two D and two A probes within the same protein complex compromises calculation of a distance with a high level of confidence.

Use of Isothermal Titration Calorimetry To Monitor the Association of the IpaB Fragments with IpgC. ITC experiments were conducted using a VP-ITC instrument (MicroCal) at 25 °C. To study the interaction between IpgC and IpaB$^{1.226}$, 30 injections of 6 μL of IpaB$^{1.226}$ (600 μM) were titrated into 1.456 mL of IpgC (30 μM). Experiments that aimed to study the interaction between IpgC and IpaB$^{28.226}$ were performed in a similar manner, except that 17 injections of 6 μL of IpaB$^{28.226}$ (1.569 mM) were titrated into 1.456 mL of IpgC (48 μM). Each set of experiments was performed in triplicate, and the final values are derived from the average of all three runs per experiment. A single-site binding model was used to fit the corrected binding isotherm and derive the thermodynamic binding parameters using Origin (OriginLab).

Cross-Linking of Different IpaB Fragments and IpgC. Copurified IpaB$^{1.94}$−IpgC and IpaB$^{1.226}$−IpgC complexes (10 μM in PBS at pH 7.4) were subjected to cross-linking using a final dithiobis(succinimidyl propionate) (DSP, a thiol-containing homobifunctional cross-linker) concentration of 168 μM.[16] After 30 min at room temperature, the reaction was quenched with sodium dodecyl sulfate−polyacrylamide gel electrophoresis (SDS−PAGE) sample buffer without reducing agents. The reaction mixtures were split into two aliquots with one aliquot receiving DTT to a final concentration of 1 mM to promote cleavage of the cross-linker. The samples were boiled, and the proteins were separated on a 17% SDS−PAGE gel and then stained with Oriole UV-fluorescent gel stain (Bio-Rad). The interaction between individually purified IpaB$^{28.226}$ or IpaB$^{1.226}$ and IpgC at a molar ratio of 1:2 was examined in a similar manner except the proteins were allowed to interact for 1 h prior to being cross-linked for 30 min. These reconstituted complexes were analyzed on 15% SDS−PAGE gels.

RESULTS

Identification, Structure, and Analysis of Stable IpaB Fragments. We previously identified stable fragments of IpaB based on limited proteolysis of the IpaB−IpgC complex (Figure S1 of the Supporting Information).[18] One IpaB fragment containing residues 28−226 (IpaB$^{28.226}$) was found to be highly soluble and stable, even in the absence of chaperone. This fragment was used to provide the first high-resolution structure for a significant portion of IpaB [residues 74−224 were resolved in this crystal structure (see Figure 1)].[18] IpaB$^{74.226}$ formed a highly stable, extended (>100 Å) coiled coil that shares exceptional structural homology with the coiled-coil region of colicins E3 and Ia.[18,25,26] Within the context of full-length IpaB, the coiled coil is immediately followed by a hydrophobic region (a functional schematic for IpaB is shown in Figure S2 of the Supporting Information). This presumably allows the IpaB N-terminal domain to present the region needed for membrane penetration outward from the T3SA needle tip.[27−29]

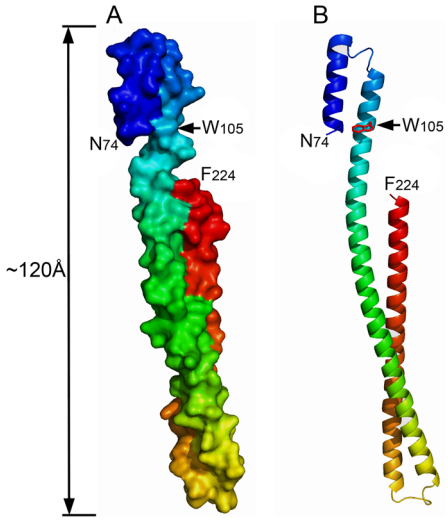

Figure 1. Crystal structure of the N-terminal domain of IpaB showing a 2.1 Å resolution for residues 74−224. The native Trp residue within this domain is identified, and Cys residues placed at the N- or C-terminus of IpaB$^{1.226}$ and IpaB$^{28.226}$ would not be visible in this structure, indicating that they are in unstructured regions within the otherwise stable N-terminal domain. Panel A shows a surface rendition of the structure (Protein Data Bank entry 3U0C), and panel B shows a ribbon depiction for this region of IpaB.[18] The position of Trp residue 105 is indicated with an arrow (W105), and the length of the entire structure is indicated.

Because IpaB N-terminal fragments copurified with IpgC, we elected to examine IpaB$^{1.226}$, IpaB$^{28.226}$, and IpaB$^{1.94}$ for their solution properties and their ability to interact with IpgC in vitro and in vivo. IpaB$^{1.226}$ was stably expressed and purified both independently and in complex with IpgC with little to no degradation occurring during the time line of this study. It is noteworthy that IpaB$^{28.226}$ contains the previously reported IpgC binding site,[12,30] but the copurified complex does not remain stably associated during further chromatographic purification steps (data not shown). Thus, no data pertaining to copurified IpaB$^{28.226}$ and IpgC could be obtained for this study. In contrast, IpaB$^{1.94}$ could be purified stably as a complex with IpgC, but was quickly degraded when expressed in the absence of IpgC. Because of this, only data pertaining to the IpaB$^{1.94}$−IpgC complex are presented here. Despite these limitations, all three IpaB N-terminal fragments, alone or in complex with IpgC, provided a platform for examining the influence of IpgC binding on the structural features of the IpaB N-terminal domain and, conversely, the influence of this region on the oligomeric state of IpgC.

Secondary Structure Analysis Reveals Stable, Highly α-Helical Polypeptides. Far-UV circular dichroism (CD) spectroscopy was first used to determine the secondary structure content and stability of the IpaB N-terminal fragments examined in this study. Previous crystallographic analysis of IpgC and IpaB$^{74.224}$ has demonstrated that both proteins are rich in α-helical structure.[12,13,18] Likewise, the CD spectra for

IpaB$^{1.94}$, IpaB$^{1.226}$, and IpaB$^{28.226}$ alone or in complex with IpgC indicate that these proteins contain a significant proportion of α-helical structure (interference below 200 nm prevented determination of secondary structure ratios) (Figure S3A of the Supporting Information).

To further analyze the solution properties of the IpaB N-terminal fragments, the thermal unfolding profiles for these polypeptides alone and in complex with IpgC were determined by monitoring the increase in the intensity of the signal for the dominant α-helix minimum at 222 nm (Table 1 and Figure S3B of the Supporting Information). IpgC exhibited a midpoint of thermal unfolding near 45 °C, while IpaB$^{1.226}$ and IpaB$^{28.226}$ unfolded at slightly higher temperatures. The IpaB$^{1.226}$–IpgC complex displayed two thermal transitions at 45 and 60 °C, perhaps indicating separation of the complex at a lower temperature followed by individual unfolding of IpgC and IpaB$^{1.226}$ at respective higher melting temperatures. Interestingly, the IpaB$^{1.94}$–IpgC complex had a thermal unfolding transition at 62.5 °C, suggesting that strong interactions occur between the extreme N-terminus of IpaB and the IpgC chaperone. These data indicate that association of the IpaB N-terminal fragments with the chaperone IpgC influences the solution properties of both proteins.

Table 1. Thermal Unfolding Temperatures for Different IpaB N-Terminal Domain Proteins with and without IpgC[a]

protein	T_m (°C)[b]
IpgC	45.0
IpaB$^{28.226}$	57.5
IpaB$^{1.226}$	57.5
IpaB$^{1.226}$–IpgC	45.0/60.0[c]
IpaB$^{1.94}$–IpgC	62.5

[a]The CD signal at 222 nm was monitored for each protein as a function of temperature from 10 to 85 °C. Spectra were collected every 2.5 °C with 5 min allowed for temperature equilibration. [b]The midpoint of thermal unfolding (given as T_m) was determined as an indicator of the transition from a folded to unfolded state. The standard error in each case is <2 °C. [c]This protein pair appeared to have two unfolding transitions, which in this case could represent a separation of the two proteins followed by observation of their individual unfolding transitions.

IpaB$^{1.226}$ and IpaB$^{28.226}$ Interact with IpgC in Vitro. Following co-expression in *E. coli*, full-length IpaB (580 residues) copurifies with IpgC, and this is the only reliable method for purifying this hydrophobic translocator protein.[16] Once IpaB is separated from IpgC by the addition of detergent, it forms stable multimers, which do not allow the re-formation of the IpaB–IpgC complex in vitro (data not shown). Therefore, we chose to determine whether the soluble IpaB N-terminal domain could be prepared alone and then used to form a complex with IpgC in vitro. Fluorescence polarization (FP) was used to monitor protein–protein interactions between unlabeled IpgC and IpaB N-terminal fragments labeled with fluorescein maleimide (FM) on a Cys residue placed at the N- or C-terminus of the IpaB fragment (FM-IpaB$^{N1.226}$, FM-IpaB$^{C1.226}$, FM-IpaB$^{N28.226}$, and FM-IpaB$^{C28.226}$). Upon addition of IpgC to the labeled IpaB N-terminal fragment, a sharp rise in polarization was seen (Figure 2). On the basis of the observed binding curves, apparent K_d values were estimated to be in the submicromolar range (Table 2), consistent with a strong interaction between these binding partners. These K_d values are based on a single-site saturation ligand binding equation, which fits well to the obtained FP data with a correlation coefficient of ≥0.94 in all cases. Comparison of the estimated K_d values suggests that the interaction between IpaB$^{1.226}$ and IpgC is stronger than that observed between IpaB$^{28.226}$ and IpgC, regardless of whether the FM is located at the N- or C-terminus. These data indicate that the extreme N-terminus of IpaB has an important role in this translocator's

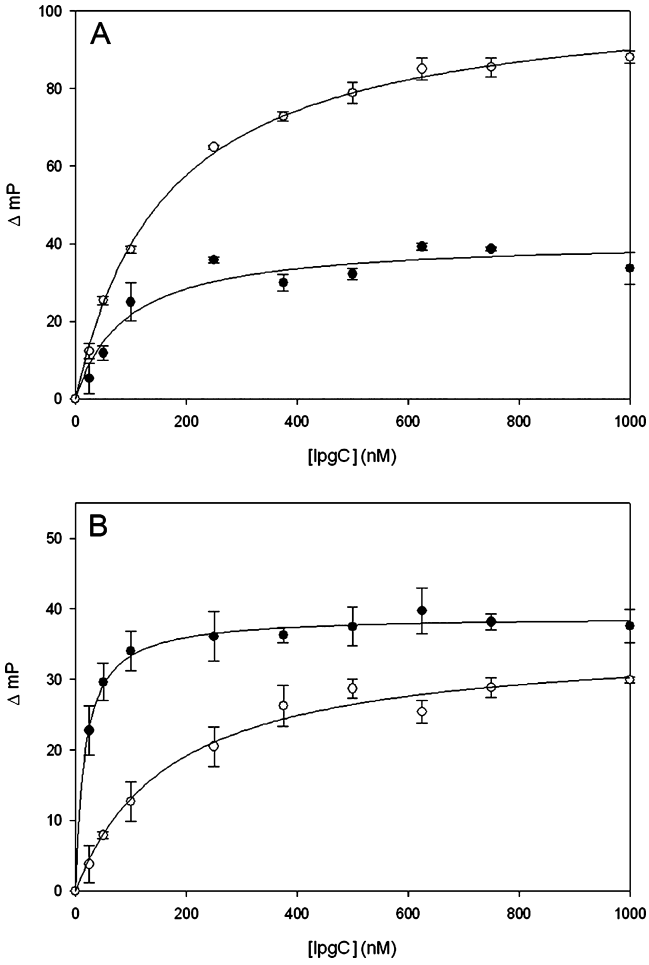

Figure 2. Fluorescence polarization (FP) measurements for the binding of IpaB$^{1.226}$ and IpaB$^{28.226}$. (A) N-Terminally FM-labeled IpaB$^{N28.226}$ (○; R^2 = 0.99) and IpaB$^{N1.226}$ (●; R^2 = 0.94) or (B) C-terminally FM-labeled IpaB$^{C28.226}$ (○; R^2 = 0.99) and IpaB$^{C1.226}$ (●; R^2 = 0.99) were held at a constant concentration as increasing concentrations of IpgC were added. A single-site ligand binding saturation equation was fit to these data. Data shown are representative of three independent experiments with at least three technical replicates per experiment. Error bars represent the standard deviation.

Table 2. Calculated Dissociation Constants for N-Terminal IpaB Fragments with IpgC Based on Fluorescence Polarization

protein	K_d (nM)[a]
IpaB$^{N28.226}$	410.9 ± 14.2
IpaB$^{C28.226}$	500.7 ± 77.1
IpaB$^{N1.226}$	199.4 ± 62.6
IpaB$^{C1.226}$	59.5 ± 5.6

[a]Dissociation constants were determined for the different protein interactions by fitting the data with a single-site saturation ligand binding algorithm using SigmaPlot.

dx.doi.org/10.1021/bi300243z | *Biochemistry* 2012, 51, 4062–4071

association with IpgC and that the extreme N-terminus, though not physically present in the published crystal structure of the IpaB N-terminal domain, is required for maximal binding affinity.

Isothermal Titration Calorimetry (ITC) Demonstrates both Endothermic and Entropically Driven Interaction between the Translocator and Chaperone. While the K_d can be calculated with isothermal titration calorimetry (ITC) or FP data, ITC has the added advantage of being fluorophore-independent as well as deriving several other relevant binding parameters (stoichiometry, ΔH, and ΔS). Therefore, we used ITC to examine the interaction between translocator fragments and the cognate chaperone (Table 3). The K_d for the interaction between IpaB$^{1.226}$ and IpgC as determined by ITC was 208 ± 51 nM, which agrees well with the K_d values obtained from the FP data (Tables 2 and 3). Likewise, reduced affinity (nearly 14-fold) was seen on the basis of the K_d value for binding of IpaB$^{28.226}$ to IpgC (K_d = 2.96 ± 0.5 μM) relative to the binding of IpaB$^{1.226}$. This is largely in agreement with the FP data presented above (Figures 2 and 3 and Tables 2 and 3). The positive ΔS and ΔH values associated with both interactions (Table 3) indicate that they are endothermic and entropically driven in nature. Significantly, both of the IpaB polypeptides associate with IpgC at an approximately equimolar ratio (Table 3). These and the FP data indicate not only that the IpaB N-terminal domain can reversibly associate with IpgC but also that the interaction occurs at an equimolar ratio and is dependent upon the N-terminus of IpaB for maximal affinity.

Table 3. Thermodynamic Parameters for the Binding of Different IpaB N-Terminal Domain Fragments with IpgC[a]

parameter	IpaB$^{1.226}$	IpaB$^{28.226}$
N^b	1.03 ± 0.01	0.88 ± 0.02
ΔH (kcal/mol)	8.68 ± 0.14	3.55 ± 0.11
ΔS (J/K)	59.7	37.2
K_d^c (μM)	0.208 ± 0.05	2.96 ± 0.53

[a]Thermodynamic parameters of the indicated protein interactions as measured by isothermal titration calorimetry. Data were fit to a single-site model to determine the binding properties. [b]N indicates the approximate stoichiometry for the IpaB N-terminal domain with IpgC. [c]K_d is the determined dissociation constant.

Cross-Linking Analyses Show That the IpaB N-Terminal Domain Associates with IpgC To Form a Heterodimer. Previously reported data have indicated that IpgC exists as a homodimer in solution.[13] There are, however, conflicting data about whether IpgC is a monomer[16] or dimer[12,17] upon association with either translocator (IpaB or IpaC). Because the ITC data presented above suggest an equimolar incorporation of IpaB and IpgC into this complex, we chose to determine the final content of the IpaB N-terminal domain−IpgC complex using chemical cross-linking analysis. Similar analyses originally indicated that full-length IpaB co-expressed with IpgC bound as a 1:1 heterodimer.[16] The copurified IpaB$^{1.226}$−IpgC cross-linked product migrated with an apparent molecular mass near 40 kDa, which agrees with the expected molecular mass for an IpaB$^{1.226}$−IpgC heterodimer (42.9 kDa) (Figure 4A). Similarly, the cross-linked, copurified IpaB$^{1.94}$−IpgC complex migrated at a molecular mass of 25 kDa, which is also consistent with heterodimer formation. The apparent molecular masses of these cross-linked complexes are

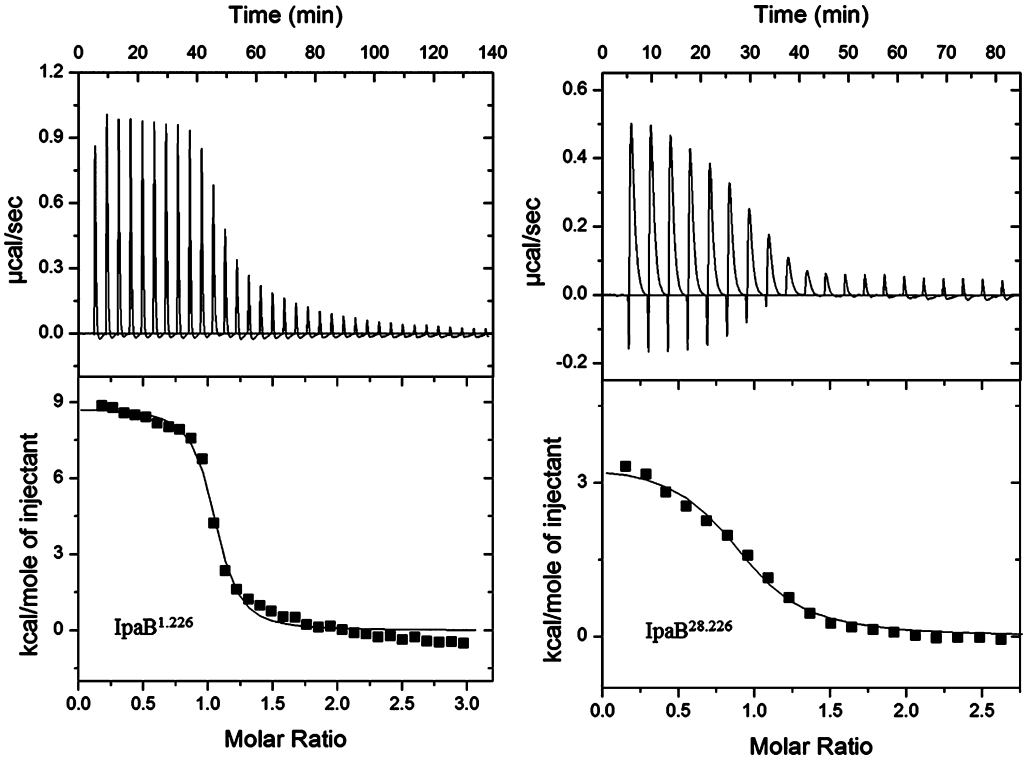

Figure 3. Isothermal titration calorimetry (ITC) measurements for IpgC and IpaB fragments. Titrations of IpgC with IpaB$^{1.226}$ (left) and IpaB$^{28.226}$ (right) as monitored by ITC. The top panel of each section depicts the thermograms obtained during the course of each injection series. The corresponding integrated enthalpy changes (after background correction) are shown in each bottom panel. A solid line that fits the data according to a single-site binding model is depicted in the bottom panel. Experimentally derived thermodynamic values are listed in Table 3.

dx.doi.org/10.1021/bi300243z | *Biochemistry* 2012, 51, 4062−4071

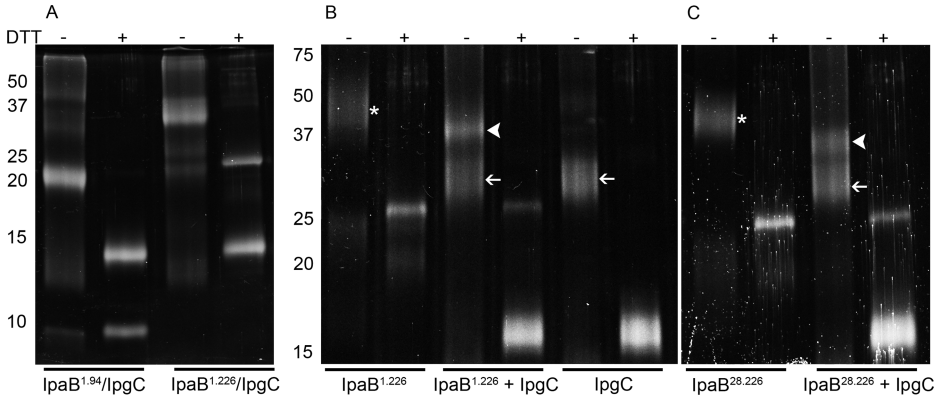

Figure 4. Chemical cross-linking analysis of the IpaB N-terminal domain and IpgC. Aliquots of protein (10 μM) were exposed to 168 μM cross-linking agent DSP at room temperature for 30 min. Cross-linking was quenched by the addition of a third volume of 3× SDS–PAGE sample buffer. The presence or absence of DTT in the sample buffer is indicated at the top of the gels. In panel A, IpaB$^{1.94}$ and IpaB$^{1.226}$ were co-expressed and copurified with IpgC followed by cross-linking as described above. In panel B, IpgC and IpaB$^{1.226}$ were expressed and purified independently. Proteins were cross-linked at IpaB:IpgC molar ratios of 0:1, 1:2, and 1:0. In panel C, IpaB$^{28.226}$ was tested at a 0- or 2-fold molar excess of IpgC. White arrowheads show the position of the IpaB–IpgC homodimer; thin white arrows show the positions of IpgC homodimers, and asterisks indicate the positions of IpaB N-terminal domain homodimers. Addition of DTT cleaves the DSP cross-linker, resulting in the formation of modified monomeric proteins.

consistent with the 1:1 stoichiometry observed using ITC and our previous report of a 1:1 stoichiometry for copurified heterodimers of these IpgC–translocator complexes (whether IpaB or IpaC).[16] When recombinant IpgC was cross-linked and evaluated, a distinct band at 35 kDa was observed. This confirmed that IpgC alone does form a homodimer in solution (Figure 4B), which is consistent with our previous reports as well as others.[12,13,16]

To complement the complexes that were formed in vivo during co-expression, we examined those that were formed by reconstituting the fragments in vitro, which cannot be accomplished with the multimerized full-length IpaB. Because IpaB$^{1.94}$ could not be prepared in the absence of IpgC, we could only examine in vitro binding between IpgC and purified IpaB$^{1.226}$ or IpaB$^{28.226}$. In accordance with a previously reported 1:2 ternary complex (one IpaB peptide with two IpgC molecules),[17] each of our IpaB N-terminal fragments was mixed with IpgC at a molar ratio of 1:2 (IpaB fragment:IpgC); however, this led to the formation of cross-linked complexes that migrated at two distinct molecular masses (Figure 4B,C). The smaller of these bands in each case corresponded to an IpgC homodimer (35 kDa) while the other to the expected mass of an IpaB fragment–IpgC heterodimer, 40 kDa for the IpaB$^{1.226}$–IpgC heterodimer and 38 kDa for the IpaB$^{28.226}$–IpgC heterodimer (Figure 4B,C). Interestingly, both IpaB N-terminal fragments appeared to form cross-linkable dimers in the absence of IpgC (Figure 4B,C). In all cases, the higher-order complexes could be separated into their component proteins by adding DTT (Figure 4). It thus appears that when the IpaB N-terminal domain dimers are mixed with the IpgC dimers, they dissociate in favor of forming an IpaB fragment–IpgC heterodimer.

It is worth noting that the heterodimers formed between the IpaB fragments and IpgC are actually smaller than the respective IpaB fragment homodimers, yet FP measurements using probes at the N- and C-termini of IpaB gave rise to an increase in polarization. This is consistent with two different possibilities. First, these regions may be held more rigidly in the IpaB fragment–IpgC complex than in the IpaB N-terminal domain homodimer. Second, during the FP experiments, this restriction overcomes the decrease in overall molecular volume caused by the transition from an IpaB domain homodimer to an IpaB–IpgC heterodimer. Because the N- and C-termini could not be modeled in the crystal structure of IpaB$^{28.226}$, they appear to be unstructured regions that perhaps gain some measure of structure upon chaperone binding. This phenomenon may very well account for the inherent instability of IpaB$^{1.94}$ in the absence of IpgC. In contrast, the Trp residue at position 105 of IpaB (W105) is contained within the core structure of IpaB$^{28.226}$ (see Figure 1). Thus, we performed FP experiments based on intrinsic Trp fluorescence. In this case, polarization decreased upon addition of IpgC, with a nearly maximal polarization decrease occurring when the two proteins are at an approximately equimolar concentration (Figure S4 of the Supporting Information). Taken together, these data are consistent with the IpaB N-terminal domain undergoing a significant conformational change upon chaperone binding.

Förster Resonance Energy Transfer Allows Examination of Relative Probe Positions within the IpaB N-Terminal Domain. To explore the possibility of a conformational change in IpaB$^{1.226}$ or IpaB$^{28.226}$ after IpgC binding, we used Förster resonance energy transfer (FRET) between the native W105 within the stable core of the IpaB fragment and an extrinsic Alexa350 acceptor linked at the less well-characterized termini of these proteins (IpaB$^{N28.226}$ or IpaB$^{N1.226}$ and IpaB$^{C28.226}$, respectively). Unfortunately, the FRET-based distance determination for the IpaB N-terminal domain alone is complicated by the fact that IpaB$^{28.226}$ and IpaB$^{1.226}$ form homodimers in the absence of IpgC; this prevents a confident calculation of the distance between the donor and acceptor in the absence of IpgC. However, the distance from W105 to A224 is approximately 18 Å in the crystal structure (see Figure 1; Protein Data Bank entry 3U0C), which is largely in agreement with the calculated distance based on FRET in the absence of chaperone (17 Å) for IpaB$^{C28.226}$. In contrast, because we have demonstrated that this IpaB domain forms a heterodimer with IpgC (which lacks Trp residues), we were able to calculate distances from W105 to each of the IpaB domain termini when the chaperone was present (Table 4 and Figure 5).

dx.doi.org/10.1021/bi300243z | Biochemistry 2012, 51, 4062–4071

Table 4. FRET-Based Determination of Intermolecular Distances for IpaB–IpgC Complexes

	no IpgC		1 μM IpgC	
protein	FRET[a] efficiency (%)	distance (Å)[b]	FRET efficiency (%)	distance (Å)[c]
$IpaB^{N28.226}$	47.1 ± 3.2	21.4	37.9 ± 14.8	22.8
$IpaB^{C28.226}$	74.5 ± 5.9	17.6	46.1 ± 6.8	21.6
$IpaB^{N1.226}$	37.6 ± 3.3	22.8	6.5 ± 3.6	32.8

[a]FRET was measured using the intrinsic probe W105 as the donor for $IpaB^{28.226}$ or $IpaB^{1.226}$ to either an N- or C-terminal Alexa350 acceptor probe as described in Experimental Procedures. FRET efficiencies and distances were calculated using eqs 1 and 2, respectively. [b]This distance is measured with the realization that it may not precisely represent the distance separating the two probes because of homodimer formation. [c]This calculation refers to the condition under which IpaB–IpgC heterodimers are formed and should represent an accurate distance between the two probes.

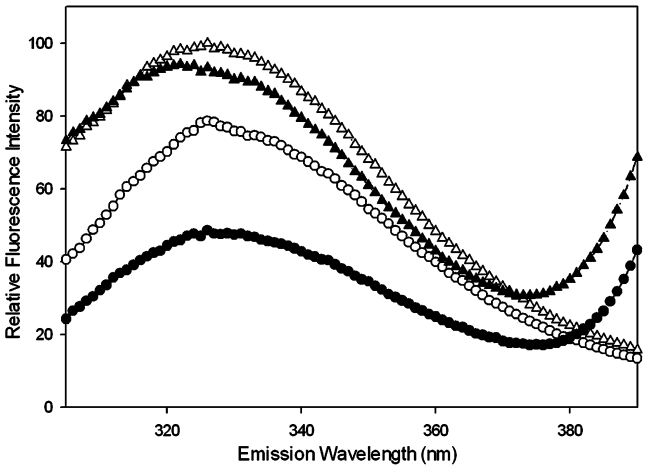

Figure 5. Use of FRET to monitor intermolecular distances during the interaction of the IpaB N-terminal domain with IpgC. Alexa350-$IpaB^{N1.226}$ (D/A) or $IpaB^{N1.226}$ (D) was excited at 295 nm, and fluorescence spectra were recorded from 300 to 400 nm in the presence and absence of 1 μM IpgC: (○) $IpaB^{N1.226}$ donor only without IpgC, (△) $IpaB^{N1.226}$ donor only with IpgC, (●) $IpaB^{N1.226}$ donor and acceptor without IpgC, and (▲) $IpaB^{N1.226}$ donor with acceptor and IpgC present. The data shown are representative of the data used to obtain the FRET efficiency values listed in Table 4. The fluorescence spectra shown here are normalized relative to the $IpaB^{N1.226}$ donor only in the presence of IpgC.

The distance from W105 to Alexa350 in $IpaB^{C28.226}$ was calculated to be 21.6 Å in the presence of an equimolar concentration of IpgC. This is an increase from the value of 18 Å predicted in the crystal structure, perhaps indicating that a modest conformational rearrangement has occurred upon association with IpgC. Because the crystal structure of the IpaB N-terminal domain does not include residues 1–73, the distances between W105 and Alexa350 at the N-termini of $IpaB^{1.226}$ and $IpaB^{28.226}$ could not be determined on the basis of static structure. Nevertheless, we were able to use FRET to calculate the distances from W105 to Alexa350 on $IpaB^{N28.226}$ or $IpaB^{N1.226}$ after the addition of IpgC. For the $IpaB^{N1.226}$–IpgC heterodimer, the distance from W105 to the N-terminal Alexa350 acceptor was calculated to be 32.8 Å. This represents a significant decrease in FRET efficiency relative to that of $IpaB^{N1.226}$ alone (from 38 to ~7%). Meanwhile, the equivalent distance for $IpaB^{N28.226}$ with IpgC was 22.8 Å, which was calculated from a FRET efficiency of 38% and did not differ substantially from the FRET efficiency seen in the absence of IpgC (Table 4). It is important to state that these data cannot be used to specifically demonstrate a change in the IpaB N-terminal domain structure upon chaperone binding. However, they are nevertheless consistent with the portion of the IpaB N-terminal domain that is not visible in the published crystal structure assuming an elongated conformation upon association with IpgC.

■ DISCUSSION

We previously used controlled digestion to identify a soluble, protease-resistant core of IpaB comprised of residues 28–226 ($IpaB^{28.226}$). This region was used to determine the recently reported crystal structure of the IpaB N-terminal domain comprised of residues 74–224 to a resolution of 2.1 Å.[18] The refined structure consisted of an extended coiled coil possessing a high degree of structural homology to the extended portion of the pore-forming toxin colicin Ia.[18,25,26] Purified IpaB has been shown to penetrate liposomes to cause the release of small molecules trapped inside, while the IpaB–IpgC chaperone complex is unable to do so.[16] When co-expressed in *E. coli*, the N-terminal IpaB fragments $IpaB^{1.226}$ and $IpaB^{1.94}$ copurify with IpgC, indicating that they contain important sequences that contribute to chaperone binding. Of these three fragments, it is interesting that $IpaB^{28.226}$ associates with IpgC when the two are co-expressed, but the two separate during the extensive purification steps used here. Unlike full-length IpaB, however, $IpaB^{1.226}$ and $IpaB^{28.226}$ can be purified in the absence of IpgC and remain soluble in the absence of detergents. In this study, we demonstrate three points. (1) The N-terminal IpaB fragments strongly interact with IpgC in vitro in a manner that supports a two-chaperone binding site model. (2) The IpaB fragment–IpgC complex is a heterodimer whose formation is more favorable than maintenance of the IpaB N-terminal domain and IpgC homodimers. (3) Upon association of IpgC, the N-terminal IpaB fragment probably undergoes a conformational change into what may be a more elongated structure.

ITC and FP data show that the binding affinity of IpgC for $IpaB^{1.226}$ is stronger than that for binding of IpgC to $IpaB^{28.226}$ alone (Figures 2 and 3 and Tables 2 and 3). It has been suggested that there are two chaperone binding domains (CBD) in IpaB, with CBD 1 being close to the N-terminus at residues 16–35 and CBD 2 located just downstream between residues 51 and 70.[12,17] Thus, when the IpaB N-terminal fragment lacks CBD 1 as is the case for $IpaB^{28.226}$, the binding affinity for IpgC is reduced relative to that seen when CBD 1 and 2 are present as in $IpaB^{1.226}$ (Figures 3 and 4 and Table 3). These data firmly support a two-site model for chaperone binding by IpaB. Structural information remains lacking for this region of IpaB, which is consistent with the N-terminal fragment of $IpaB^{1.94}$ being rapidly degraded in the absence of IpgC. In contrast, $IpaB^{1.94}$ is quite stable as part of the complex with IpgC but is unstable and thus may be largely unstructured in the absence of a chaperone. When all the data are considered, it would seem that residues within this region have a significant role in directing binding of IpaB to IpgC. This could explain why the $IpaB^{28.226}$–IpgC complex dissociates during the purification process while the $IpaB^{1.226}$–IpgC complex remains intact.

Cross-linking experiments showed that IpgC and the IpaB N-terminal fragments form homodimers in solution and that

incubating these two sets of homodimers with each other in vitro leads to the formation of IpaB fragment−IpgC heterodimers. It thus appears that the IpaB N-terminal domain and IpgC homodimers dissociate in favor of forming IpaB−IpgC heterodimers in solution. These results are consistent with the ITC data demonstrating a 1:1 stoichiometry. Furthermore, size exclusion chromatography elution profiles of IpaB$^{1.226}$ and copurifed IpaB$^{1.226}$−IpgC heterodimers demonstrate distinct molecular sizes that are consistent with stable homodimer and heterodimer formation, respectively (data not shown). While others have suggested that the association of the IpaB−IpgC complex occurs in a 1:2 ratio,[12,17] the current results are supported and complemented by our previous co-expression and copurification of IpgC−IpaB or IpgC−IpaC complexes.[16] Using the same cross-linking methodology as well as analytical ultracentrifugation, we demonstrated that IpgC complexes with full-length IpaB and IpaC exist as 1:1 heterodimers.[16]

The FRET experiments presented here suggest that the extreme N-terminus of IpaB adopts an extended conformation when it binds to IpgC. While such data are only suggestive that an actual conformational change occurs in the IpaB N-terminal domain upon association with IpgC, they are consistent with the unstructured region of the N-terminus becoming elongated as a result of chaperone binding. When those results are considered in the overall context of the findings presented here, however, there is good evidence that the N-terminus of IpaB is unstructured and association with IpgC has a major impact on the conformation that it finally assumes. This is not unlike what has been shown for other T3SS effectors such as SptP.[31] For example, the FP data indicate that N- and C-terminal probes become restrained in motion upon IpgC binding (based on an increase in the mP value), despite the fact that conversion from an IpaB fragment homodimer to an IpaB−IpgC heterodimer reduces the overall size of the complex. This suggests that the termini become more rigid upon chaperone binding. In contrast, W105 displays reduced polarization when IpaB associates with IpgC, which could be a reflection of either the reduced size of the heterodimer or an increase in local flexibility upon association with IpgC.

The ITC data obtained here provide important insight into the thermodynamics of formation of translocator−chaperone heterodimers from two individual homodimers. In addition to measuring the binding affinity (K_d) between a chaperone and a translocator, we found both enthalpy (ΔH) and entropy (ΔS) data suggest the forces that drive complex formation and the events involved in this process.[32] For example, the thermodynamic parameters reported here reveal that both IpaB$^{1.226}$ and IpaB$^{28.226}$ bind to IpgC in an endothermic, entropy-driven manner (Table 3). This entropically favorable reaction directly correlates to the change in higher-order structure (here shown as the dissociation of two homodimers to allow the formation of two separate heterodimers). While the change in enthalpy for the IpaB$^{28.226}$−IpgC interaction (ΔH = 3.55 ± 0.11 kcal/mol) was smaller than the measured value for the IpaB$^{1.226}$−IpgC interaction (ΔH = 8.68 ± 0.14 kcal/mol), both were found to be endothermic and are likely to reflect disruption of the IpaB and IpgC homodimer contacts and displacement of the ordered solvent from the proteins' surface. This is further supported by the significant increases in entropy for both interactions (ΔS = 59.7 and 37.2 J/K for IpaB$^{1.226}$ and IpaB$^{28.226}$, respectively). It is not surprising to find that the formation of the heterodimeric IpaB fragment−IpgC complex is thermodynamically spontaneous in vitro as the ATPase located at the T3SA cytoplasmic face is likely required for disruption of this stable complex in vivo.[33]

Much remains to be learned about the roles of translocator proteins in T3SS function. The *Shigella* T3SA continues to be an important model system in understanding type III secretion and, in particular, for dissecting the steps that bridge T3SA assembly and T3SS induction. Prior to mobilization of IpaB to the needle tip complex, this protein is stored in the bacterial cytoplasm where it associates as a heterodimer with its cognate chaperone IpgC. This is a stable complex, which appears to require the active participation of an ATPase at the cytoplasmic face of the T3SA for separation. Once separated, IpaB adopts a conformation at the T3SA needle tip that is compatible with its new role as a sensor of host cell (membrane) contact and, later, as an essential translocon pore component. This requires that new sets of protein−protein interactions form. On the other hand, IpgC remains in the bacterial cytoplasm where it forms a homodimer that may be shunted off to assume new roles in type III secretion. It is possible that the IpgC homodimer is now able to bind to the transcriptional regulator MxiE to promote the expression of late effector genes.[34] Further exploration of the temporal interactions that occur for IpaB and IpgC is clearly warranted to improve our understanding of the early interactions that ultimately allow *Shigella* to invade human intestinal epithelial cells. This work and additional structural analysis of IpaB and IpgC are steps in developing a complete understanding of the induction of type III secretion.

■ ASSOCIATED CONTENT

Supporting Information

Proteolysis data used to derive the protein fragments used in this paper (primarily IpaB$^{28.226}$) and for prior crystallographic analysis (Figure S1), a schematic of the functional organization of IpaB (Figure S2), full CD spectra and thermal folding profiles for each protein used in this study (Figure S3), and fluorescence polarization data acquired using the native Trp in the IpaB N-terminal domain (Figure S4). This material is available free of charge via the Internet at http://pubs.acs.org.

■ AUTHOR INFORMATION

Corresponding Author

*W.L.P.: Department of Microbiology and Molecular Genetics, Oklahoma State University, 307 Life Sciences East, Stillwater, OK 74078; e-mail, wendy.picking@okstate.edu; telephone, (405) 744-4600. W.D.P.: Department of Microbiology and Molecular Genetics, Oklahoma State University, 307 Life Sciences East, Stillwater, OK 74078; e-mail, william.picking@okstate.edu; telephone, (405) 744-6243.

Author Contributions

P.R.A. and M.K.P. contributed equally to this work.

Funding

†This work was supported by funding to W.L.P. [National Institutes of Health (NIH) Grant R01 AI067858], W.D.P. (Oklahoma Health Research Program Funding HR10-128S), and W.D.P. and B.V.G. (NIH Grant R21 AI090149). M.K.P. was supported by the Oklahoma State University Niblack Research Scholars Program.

Notes

The authors declare no competing financial interest.

■ ACKNOWLEDGMENTS

We gratefully acknowledge technical assistance from Kirk Pendleton and Daniel R. Picking.

■ ABBREVIATIONS

T3SS, type III secretion system; T3SA, type III secretion apparatus; Ipg, invasion plasmid gene; Ipa, invasion plasmid antigen; Mxi, major exporter of Ipas; CD, circular dichroism; FM, fluorescein maleimide; FP, fluorescence polarization; mP, millipolarization units; Alexa350, Alexa-Fluor 350 maleimide; FRET, Förster resonance energy transfer; ITC, isothermal titration calorimetry; TCEP, tris(2-carboxyethyl)phosphine; DSP, dithiobis(succinimidyl proprionate); DMSO, dimethyl sulfoxide; DMF, *N*′,*N*′-dimethylformamide; TPR, tetratricopeptide repeat; T_m, thermal unfolding midpoint; $IpaB^{N28.226}$ and $IpaB^{C28.226}$, N- and C-terminal Cys of $IpaB^{28.226}$, respectively; $IpaB^{N1.226}$ and $IpaB^{C1.226}$, N- and C-terminal Cys of $IpaB^{1.226}$, respectively.

■ REFERENCES

(1) Mueller, C., Broz, P., and Cornelis, G. (2008) The type III secretion system tip complex and translocon. *Mol. Microbiol. 68*, 1085−1095.

(2) Cornelis, G. R. (2010) The type III secretion injectisome, a complex nanomachine for intracellular 'toxin' delivery. *Biol. Chem. 391*, 745−751.

(3) Schroeder, G. N., and Hilbi, H. (2008) Molecular pathogenesis of *Shigella* spp.: Controlling host cell signaling, invasion, and death by type III secretion. *Clin. Microbiol. Rev. 21*, 134−156.

(4) Espina, M., Olive, A. J., Kenjale, R., Moore, D. S., Ausar, S. F., Kaminski, R. W., Oaks, E. V., Middaugh, C. R., Picking, W. D., and Picking, W. L. (2006) IpaD Localizes to the Tip of the Type III Secretion System Needle of *Shigella flexneri*. *Infect. Immun. 74*, 4391−4400.

(5) Darboe, N., Kenjale, R., Picking, W. L., Picking, W. D., and Middaugh, C. R. (2006) Physical characterization of MxiH and PrgI, the needle component of the type III secretion apparatus from *Shigella* and *Salmonella*. *Protein Sci. 15*, 543−552.

(6) Blocker, A., Jouihri, N., Larquet, E., Gounon, P., Ebel, F., Parsot, C., Sansonetti, P., and Allaoui, A. (2001) Structure and composition of the *Shigella flexneri* "needle complex", a part of its type III secreton. *Mol. Microbiol. 39*, 652−663.

(7) Veenendaal, A. K., Hodgkinson, J. L., Schwarzer, L., Stabat, D., Zenk, S. F., and Blocker, A. J. (2007) The type III secretion system needle tip complex mediates host cell sensing and translocon insertion. *Mol. Microbiol. 63*, 1719−1730.

(8) Epler, C. R., Dickenson, N. E., Bullitt, E., and Picking, W. L. (2012) Ultrastructural Analysis of IpaD at the Tip of the Nascent MxiH Type III Secretion Apparatus of *Shigella flexneri*. *J. Mol. Biol.*, DOI: 10.1016/j.jmb.2012.03.025.

(9) Olive, A. J., Kenjale, R., Espina, M., Moore, D. S., Picking, W. L., and Picking, W. D. (2007) Bile salts stimulate recruitment of IpaB to the *Shigella flexneri* surface, where it colocalizes with IpaD at the tip of the type III secretion needle. *Infect. Immun. 75*, 2626−2629.

(10) Epler, C. R., Dickenson, N. E., Olive, A. J., Picking, W. L., and Picking, W. D. (2009) Liposomes recruit IpaC to the *Shigella flexneri* type III secretion apparatus needle as a final step in secretion induction. *Infect. Immun. 77*, 2754−2761.

(11) Parsot, C., Hamiaux, C., and Page, A. L. (2003) The various and varying roles of specific chaperones in type III secretion systems. *Curr. Opin. Microbiol. 6*, 7−14.

(12) Lunelli, M., Lokareddy, R. K., Zychlinsky, A., and Kolbe, M. (2009) IpaB-IpgC interaction defines binding motif for type III secretion translocator. *Proc. Natl. Acad. Sci. U.S.A. 106*, 9661−9666.

(13) Barta, M. L., Zhang, L., Picking, W. L., and Geisbrecht, B. V. (2010) Evidence for alternative quaternary structure in a bacterial type III secretion system chaperone. *BMC Struct. Biol. 10*, 21.

(14) Büttner, C., Sorg, I., Cornelis, G., Heinz, D., and Niemann, H. (2008) Structure of the *Yersinia enterocolitica* type III secretion translocator chaperone SycD. *J. Mol. Biol. 375*, 997−1012.

(15) Job, V., Mattei, P., Lemaire, D., Attree, I., and Dessen, A. (2010) Structural basis of chaperone recognition of type III secretion system minor translocator proteins. *J. Biol. Chem. 285*, 23224−23232.

(16) Birket, S. E., Harrington, A. T., Espina, M., Smith, N. D., Terry, C. M., Darboe, N., Markham, A. P., Middaugh, C. R., Picking, W. L., and Picking, W. D. (2007) Preparation and characterization of translocator/chaperone complexes and their component proteins from *Shigella flexneri*. *Biochemistry 46*, 8128−8137.

(17) Lokareddy, R. K., Lunelli, M., Eilers, B., Wolter, V., and Kolbe, M. (2010) Combination of two separate binding domains defines stoichiometry between type III secretion system chaperone IpgC and translocator protein IpaB. *J. Biol. Chem. 285*, 39965−39975.

(18) Barta, M. L., Dickenson, N. E., Patil, M., Keightley, A., Wyckoff, G. J., Picking, W. D., Picking, W. L., and Geisbrecht, B. V. (2012) The Structures of Coiled-Coil Domains from Type Three Secretion System Translocators Reveal Homology to Pore-Forming Toxins. *J. Mol. Biol. 417*, 395−405.

(19) Geisbrecht, B., Bouyain, S., and Pop, M. (2006) An optimized system for expression and purification of secreted bacterial proteins. *Protein Expression Purif. 46*, 23−32.

(20) Garcia, B. L., Summers, B. J., Lin, Z., Ramyar, K. X., Ricklin, D., Kamath, D. V., Fu, Z. Q., Lambris, J. D., and Geisbrecht, B. V. (2012) Diversity in the C3B contact residues and tertiary structures of the staphylococcal complement inhibitor (SCIN) protein family. *J. Biol. Chem. 287*, 628−640.

(21) Geisbrecht, B. V., Bouyain, S., and Pop, M. (2006) An optimized system for expression and purification of secreted bacterial proteins. *Protein Expression Purif. 46*, 23−32.

(22) Martinez-Becerra, F. J., Kissmann, J. M., Diaz-McNair, J., Choudhari, S. P., Quick, A. M., Mellado-Sanchez, G., Clements, J. D., Pasetti, M. F., and Picking, W. L. (2012) Broadly protective *Shigella* vaccine based on type III secretion apparatus proteins. *Infect. Immun. 80*, 1222−1231.

(23) Lakowicz, J. R. (1983) *Principles of Fluorescence Spectroscopy*, Plenum Press, New York.

(24) Oyston, P. C., Mellado-Sanchez, G., Pasetti, M. F., Nataro, J. P., Titball, R. W., and Atkins, H. S. (2010) A Yersinia pestis guaBA mutant is attenuated in virulence and provides protection against plague in a mouse model of infection. *Microb. Pathog. 48*, 191−195.

(25) Wiener, M., Freymann, D., Ghosh, P., and Stroud, R. M. (1997) Crystal structure of colicin Ia. *Nature 385*, 461−464.

(26) Soelaiman, S., Jakes, K., Wu, N., Li, C., and Shoham, M. (2001) Crystal structure of colicin E3: Implications for cell entry and ribosome inactivation. *Mol. Cell 8*, 1053−1062.

(27) McGhie, E. J., Hume, P. J., Hayward, R. D., Torres, J., and Koronakis, V. (2002) Topology of the *Salmonella* invasion protein SipB in a model bilayer. *Mol. Microbiol. 44*, 1309−1321.

(28) Hume, P. J., McGhie, E. J., Hayward, R. D., and Koronakis, V. (2003) The purified Shigella IpaB and *Salmonella* SipB translocators share biochemical properties and membrane topology. *Mol. Microbiol. 49*, 425−439.

(29) Baudry, B., Kaczorek, M., and Sansonetti, P. J. (1988) Nucleotide sequence of the invasion plasmid antigen B and C genes (ipaB and ipaC) of *Shigella flexneri*. *Microb. Pathog. 4*, 345−357.

(30) Page, A., Fromont-Racine, M., Sansonetti, P., Legrain, P., and Parsot, C. (2001) Characterization of the interaction partners of secreted proteins and chaperones of *Shigella flexneri*. *Mol. Microbiol. 42*, 1133−1145.

(31) Stebbins, C. E., and Galan, J. E. (2001) Maintenance of an unfolded polypeptide by a cognate chaperone in bacterial type III secretion. *Nature 414*, 77−81.

(32) Ramirez, K., Ditamo, Y., Rodriguez, L., Picking, W. L., van Roosmalen, M. L., Leenhouts, K., and Pasetti, M. F. (2010) Neonatal

mucosal immunization with a non-living, non-genetically modified *Lactococcus lactis* vaccine carrier induces systemic and local Th1-type immunity and protects against lethal bacterial infection. *Mucosal Immunol. 3*, 159−171.
(33) Akeda, Y., and Galan, J. E. (2005) Chaperone release and unfolding of substrates in type III secretion. *Nature 437*, 911−915.
(34) Mavris, M., Page, A. L., Tournebize, R., Demers, B., Sansonetti, P., and Parsot, C. (2002) Regulation of transcription by the activity of the *Shigella flexneri* type III secretion apparatus. *Mol. Microbiol. 43*, 1543−1553.